Modelling the performance of a scroll expander for small organic Rankine cycles when changing the working fluid

Antonio Giuffrida

Politecnico di Milano – Dipartimento di Energia, Via R. Lambruschini 4, 20156 Milano, Italy

Received 15 November 2013
Accepted 3 June 2014
Available online 12 June 2014

1. Introduction

Organic Rankine cycle (ORC) has become a field of intense research in recent years as a very promising technology for conversion of heat into mechanical work or electricity [1]. Various heat sources can be considered: biomass combustion, solar radiation, ground heat or waste heat from internal combustion engines, industrial processes, etc. The working fluid is a refrigerant or a hydrocarbon, which allows exploiting even low-temperature (80–150 °C) waste and renewable heat sources. Thus, effective heat recovery from such sources could drive an increase in the market share of renewable energy systems, even based on small and micro ORC systems, which are currently at the level of laboratory prototype or under research. However, the selection of the expander is not easy, since small ORC systems are characterized by specific features such as limited flow rates of the working fluid, small flow passages and difficulty in sealing. Qiu et al. [2] gave an overview of expansion devices for micro-CHP ORC systems and concluded that both scroll and vane expanders are good choices for systems within the capacity range of 1–10 kW. In particular, scroll machines are well adapted to small-scale ORC applications and offer significant advantages such as reliability and robustness (reduced number of moving parts), simplicity (no inlet and outlet valves), as well as ability to handle high pressure ratios [3].

1.1. Scroll expanders in ORC systems

Scroll expanders are not a commercially ready technology, as the available prototypes are usually developed for the purpose of

E-mail address: antonio.giuffrida@polimi.it.

laboratory experiments by modifying a commercial scroll compressor for HVAC applications to make it run in reverse. However, on the occasion of the two recent international conferences on ORC systems in 2011 [4] and 2013 [5], presentations on small-scale systems, prototypes and scroll expanders have shown that there is potential in CHP units based on ORC technology.

Literature on scroll machines as expanders in ORC systems is very rich. With reference to the most recent works, as detailed hereafter, Declaye et al. [6] modified and experimentally characterized an air scroll compressor to operate in expander mode with HFC-245fa as working fluid in an ORC system designed for a nominal net power output of 1.8 kW. The maximum isentropic efficiency and shaft power were 75.7% and 2.1 kW, respectively. An experimental ORC system with scroll expander for heat recovery from low-temperature flue gas produced by a liquefied petroleum gas stove was constructed by Zhou et al. [7]. Under the experimental conditions, the maximum power output of the expander was 645 W, with cycle and heat recovery efficiencies equal to 8.5% and 22%, respectively. Another scroll expander was tested by Twomey et al. [8] in a small ORC system to calibrate a model similar to the one formerly proposed by Lemort et al. [9], later incorporated into a dynamic model of a solar thermal cogeneration system. According to the study, the scroll expander showed maximum isentropic efficiency and instantaneous power of 59% and 676 W, respectively. Oudkerk et al. [10] evaluated the performance of an ORC-based micro-CHP unit using a scroll expander, experimentally characterized in a previous work [3]. HFC-245fa was selected as working fluid for the ORC, exhibiting an overall electrical efficiency of about 8% and an overall thermal efficiency around 87%. In particular, by increasing the maximum fluid temperature at the expander inlet (limited to 140 °C due to technical reasons) and using two scroll expanders in series, overall electrical efficiency as high as 12.5% is reached. ORC simulations with a one-dimensional model of a scroll machine were presented by Clemente et al. [11] (i) for a bottoming cycle of a 18 kW_{el} internal combustion engine and (ii) for a low-temperature solar-based system. The same authors realized, tested and modelled a small-size ORC prototype, where the scroll expander, operating with HFC-245fa, was expected to deliver a power of about 1.5 kW [12]. A small-scale low-temperature solar ORC system powered by scroll expanders was also investigated by Kosmadakis et al. [13], focusing on some key aspects of its design and operation, in order for the system to track the optimized point under variable weather conditions. A scroll expander is the expansion machine selected for the hybrid solar-biomass ORC-based micro-CHP system proposed by Jradi and Riffat [14], with a maximum electric power generated in the range of 500 W and an isentropic efficiency up to 80%. Finally, part load operation calculations of a 5 kW_{el} ORC system are even proposed by Ibarra et al. [15], with a scroll expander modelling similarly as in Ref. [9].

1.2. Expander simulation in small ORC calculations

Technical papers dealing with small-size ORC systems do not always consider a specific modelling for the expander. As a matter of fact, there are several literature works focusing on the feasibility study of the ORC system and the selection of the proper working fluid. In such theoretical works, the expander efficiency is taken constant in spite of variable operating conditions, such as fluid pressure and temperature at the inlet of the machine, expansion pressure ratio, type of working fluid, etc. As a first example, the results of thermodynamic simulations of a 2 kW_{el} biomass-fired CHP system were presented by Liu et al. [16], assuming a constant isentropic expander efficiency equal to 85%, as suggested by Saleh et al. [17], despite such a value was originally chosen for a power output of 1 MW [17]. As a second example, twenty fluids for a solar ORC system generating 2 kW of power output were investigated by Tchanche et al. [18], with an isentropic expander efficiency fixed at 0.7. Although the last efficiency value is more realistic for a few kW-size expander, the machine is considered adiabatic and, consequently, the condenser heat duty is overestimated. As a last example, a thermodynamic criterion to select the most suitable working fluid for ORC CHP units in small households (for 3–4 kW) was proposed by Mikielewicz and Mikielewicz [19], based on an isentropic expansion.

However, there is another issue, specifically regarding the working fluid, in addition to the one related to constant expansion efficiency. As a matter of fact, researches oriented to investigate the proper fluid selection for ORC applications often propose solutions, e.g. HCFCs, that are to be phased out according to current regulations. As an example, both HCFC-123 and HCFC-141b are suggested in the relatively recent paper [19], because they allow for higher thermal efficiency. Likewise, these HCFCs are also included in the previously mentioned study by Tchanche et al. [18], as well as in very recent studies by Wang et al. [20] and by Xi et al. [21], with the latter also recommending CFC-11 for its superior thermodynamic performance.

1.3. Objective of the work

This paper proposes a performance simulation tool of a scroll expander for any working fluid, as a generalization of the model originally developed by Lemort et al. [9] employing HCFC-123. In particular, after presenting the procedure, the expander performance is simulated for some refrigerant fluids, so the new model can be used for calculations of small ORC systems.

2. Scroll expander modelling

The semi-empirical scroll expander model developed by Lemort et al. [9] is the starting point for the current study. A description of the expansion process modelling, along with the related equations, is included in this section. Fig. 1 shows the processing of the working fluid as it flows through the scroll expander in a number of hypothetical stages, from a) to g), as described hereafter.

a) Adiabatic supply pressure drop (su → su,1). This process accounts for all pressure losses between the expander inlet and the variable volume chamber. It is simulated as an isentropic flow through a converging nozzle whose cross sectional area is A_{su}:

$$\dot{m} = \rho_{su,1} \cdot A_{su} \cdot \sqrt{2 \cdot (h_{su} - h_{su,1})} \tag{1}$$

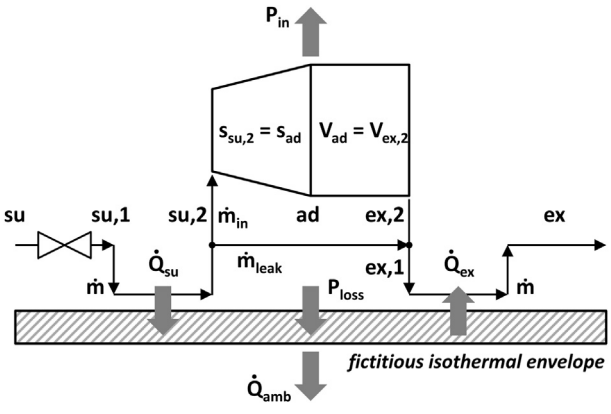

Fig. 1. Conceptual scheme of the expander model proposed by Lemort et al. [9].

Because of the steady-state nature of the model, the area A_{su} stands for an average value of the inlet port effective area over the entire supply process.

b) Isobaric supply cooling-down (su,1 → su,2). Heat transfer occurs between the fluid entering the variable volume chamber and a fictitious isothermal envelope, which is a lumped variable introduced to simulate the scrolls and the casing. Supply heat transfer is modelled as:

$$\dot{Q}_{su} = \dot{m}\cdot(h_{su,1} - h_{su,2}) = \left[1 - e^{-\frac{AU_{su}}{\dot{m}\cdot c_p}}\right]\cdot\dot{m}\cdot c_p\cdot(T_{su,1} - T_w) \tag{2}$$

The supply heat transfer coefficient AU_{su} is assumed to depend on the mass flow rate according to:

$$AU_{su} = AU_{su,nom}\cdot\left(\frac{\dot{m}}{\dot{m}_{nom}}\right)^{0.8} \tag{3}$$

where $AU_{su,nom}$ is the nominal supply heat transfer coefficient corresponding to the nominal mass flow rate. The last relationship can be justified by the Reynolds analogy for a turbulent flow [22].

c) Internal leakage (su,2 → ex,2). As schematized in Fig. 1, the mass flow rate entering the expander, according to Eq. (1), is split into two parts: the first, necessary to cause the shaft to rotate at a specified rotational speed, is related to the swept volume and the built-in volume ratio and the second is the leakage mass flow rate:

$$\dot{m} = \rho_{su,2}\cdot\frac{V_{sw}}{BVR}\cdot n + \dot{m}_{leak} \tag{4}$$

No useful expansion is related to fluid leakage through the machine, resulting in a significant loss. All leakage paths are lumped into a hypothetical area A_{leak}, which is used to simulate the leakage flow rate similarly as in Eq. (1):

$$\dot{m}_{leak} = \rho_{leak}\cdot A_{leak}\cdot\sqrt{2\cdot(h_{su,2} - h_{leak})} \tag{5}$$

i.e. the flow rate through an isentropic nozzle, whose outlet area is A_{leak}. The pressure at the inlet of this fictitious nozzle is $p_{su,2}$, whereas the outlet pressure is the highest between $p_{ex,2}$ (equal to the pressure at the expander outlet) and $p_{crit,leak}$:

$$p_{crit,leak} = p_{su,2}\cdot\left(\frac{2}{\gamma+1}\right)^{\frac{\gamma}{\gamma-1}} \tag{6}$$

which is the critical pressure [23] calculated from pressure $p_{su,2}$ by considering the working fluid as a perfect gas, with γ given by the ratio between the heat capacity at constant pressure and the heat capacity at constant volume.[1] Both ρ_{leak} and h_{leak} in Eq. (5) are calculated after the highest pressure between $p_{ex,2}$ and $p_{crit,leak}$ is determined, along with the condition $s_{leak} = s_{su,2}$.

d) Adiabatic and reversible expansion to the adapted pressure (su,2 → ad). The adapted pressure is related to the built-in volume ratio of the positive-displacement expander:

$$v_{ad} = BVR\cdot v_{su,2} \tag{7}$$

e) Adiabatic expansion at constant machine volume (ad → ex,2). As schematized in Fig. 2, under- and over-expansion losses occur at this stage, when the adapted pressure is higher or lower, respectively, than the system pressure at the expander outlet. In order to equalize these pressures, the model assumes that some fluid flows out of or into the variable volume chamber instantaneously, after the chamber opens to the outlet line and the fluid is no more trapped.

f) Adiabatic fluid mixing (ex,2 → ex,1). The mass flow rate related to shaft rotation, i.e. the first term in the right side of Eq. (4), and the leakage flow rate mix altogether, resulting in a slight increase in specific enthalpy ($h_{ex,1} > h_{ex,2}$).

g) Isobaric exhaust heating-up or cooling-down (ex,1 → ex). Heat is exchanged between the fluid exiting the expander and the fictitious isothermal envelope and is modelled similarly as in Eq. (2).

After determining the thermodynamic states, along with mass flow rates $\dot{m}$ and $\dot{m}_{leak}$, the internal expander power is formulated as

$$P_{in} = (\dot{m} - \dot{m}_{leak})\cdot\left[(h_{su,2} - h_{ad}) - v_{ad}\cdot\left(p_{ad} - p_{ex,2}\right)\right] \tag{8}$$

The mechanical power losses are lumped into a constant loss parameter, so the shaft power output is calculated as:

$$P_{sh} = P_{in} - P_{loss} = P_{in} - \frac{2\cdot\pi\cdot n}{60}\cdot\tau_{loss} \tag{9}$$

The ambient heat losses are simulated by introducing a global heat transfer coefficient AU_{amb} between the casing and the surroundings:

$$\dot{Q}_{amb} = AU_{amb}\cdot(T_w - T_{amb}) \tag{10}$$

Ultimately, the mechanical power losses are assumed to be injected directly into the envelope, so the temperature T_w is computed once the heat balance over the expander is completed as:

$$P_{loss} + \dot{Q}_{su} - \dot{Q}_{amb} \pm \dot{Q}_{ex} = 0 \tag{11}$$

where the correct sign of the last term is fixed according to the temperature difference between $T_{ex,1}$ and T_w.

As a figure of merit, the expander efficiency is defined by the ratio of the shaft power and the isentropic power:

$$\eta = \frac{P_{sh}}{\dot{m}\cdot(h_{su} - h_{ex,is})} \tag{12}$$

where $h_{ex,is}$ is calculated at pressure p_{ex} with entropy equal to s_{su}.

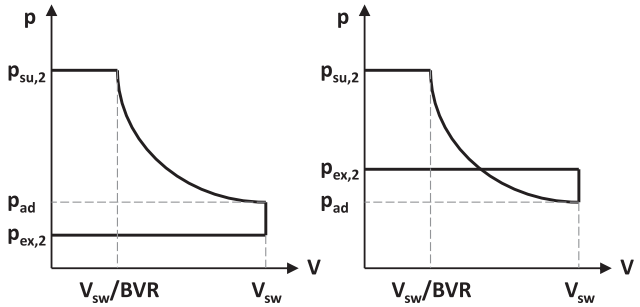

Fig. 2. Schematic under- and over-expansion processes in the p–V diagram (on the left and on the right, respectively).

[1] Referring to HCFC-123, the ratio between the heat capacity at constant pressure and the heat capacity at constant volume reduces from 1.19 to 1.13 (at 1 MPa) and from 1.11 to 1.09 (at 0.5 MPa) for temperatures ranging from 120 °C to 165 °C (superheated region).

Table 1
Model parameters of the scroll expander operating with HCFC-123 [9].

Parameter	Description	Value
$\dot{m}_{nom}$	Nominal mass flow rate	120 g s^{-1}
A_{leak}	Leakage area	4.06 mm^2
A_{su}	Supply port cross-sectional area	27.43 mm^2
$AU_{su,nom}$	Supply heat transfer coefficient	21.2 W K^{-1}
$AU_{ex,nom}$	Exhaust heat transfer coefficient	34.2 W K^{-1}
AU_{amb}	Heat transfer coefficient with the ambient	6.4 W K^{-1}
BVR	Built-in volume ratio	4.05
V_{sw}	Swept volume	147.987 cm^3
τ_{loss}	Mechanical loss torque	0.47 N m

The validation of the expander model is achieved after the values of the parameters throughout the detailed equation set are identified according to specific experimental data. In particular, Table 1 details the parameters of the scroll expander model identified by Lemort et al. [9] by minimizing a global error function accounting for the errors on the predictions of mass flow rate, shaft power and exhaust temperature, whereas Table 2 reports the range of the main variables fixed in the experimental campaign for the model validation [9].

An overview of expansion simulations based on the previously described model is shown in Figs. 3–5 that quantitatively detail three specific expansion processes in the T–s diagram: solid thick lines are here used to trace the process simulated for each expansion stage, whereas a dashed line connects the thermodynamic states of the fluid at the inlet and the outlet of the expander. In particular,

- Fig. 3 shows an over-expansion ($\beta = 3$),
- Fig. 4 shows an adapted expansion ($\beta = 4.43$),
- Fig. 5 shows an under-expansion ($\beta = 7.5$),

when feeding the expander with HCFC-123 at 1 MPa and 125 °C and the shaft rotating at 2000 rpm. Efficiency values, as calculated with Eq. (12), result equal to 56.7%, 65.6% and 63.6%, respectively.

3. Modelling the change of the working fluid

The procedure proposed to change the working fluid in the previously detailed scroll expander model operating with HCFC-123 is similar to the one proposed by Byrne et al. for a scroll compressor model adapted from HFC-407C to propane [24] and other hydrocarbons [25]. A similar approach was also adopted by Duprez et al. [26] for their improvements in scroll compressor modelling.

With reference to the parameter set reported in Table 1, it is possible to realize that A_{leak}, A_{su}, BVR, as well as the swept volume, are characteristic of the specific machine considered in the original model and do not depend on the working fluid, contrary to $AU_{su,nom}$ and $AU_{ex,nom}$, which must be re-determined. As a matter of fact, these two parameters take the heat transfer between the working fluid and the casing into account. On the other hand, the parameter

Table 2
Range of the main variables for model validation [9].

p_{su} (kPa)	545–1112
T_{su} (°C)	101.7–165.2
ΔT_{su} (K)	2.2–68.9
p_{ex} (kPa)	138–266
T_{ex} (°C)	66.4–128
n (rpm)	1771–2660
P_{sh} (W)	382–1820

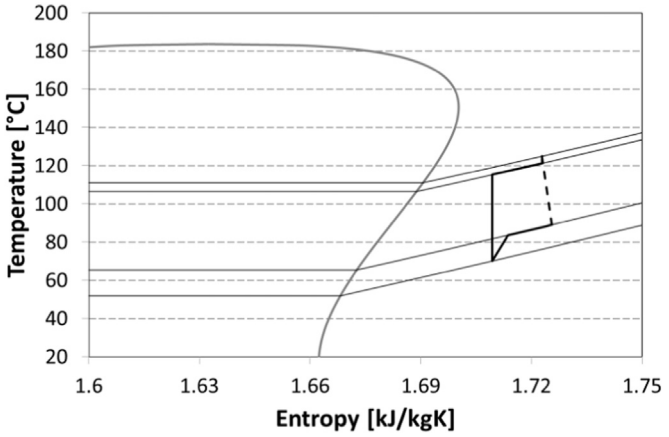

Fig. 3. T–s diagram with over-expansion of HCFC-123 ($p_{su} = 1$ MPa, $T_{su} = 125$ °C, $\beta = 3$, $n = 2000$ rpm): solid thick lines trace the process simulated for each expansion stage whereas a dashed line connects the thermodynamic states of the fluid at the inlet and the outlet of the expander.

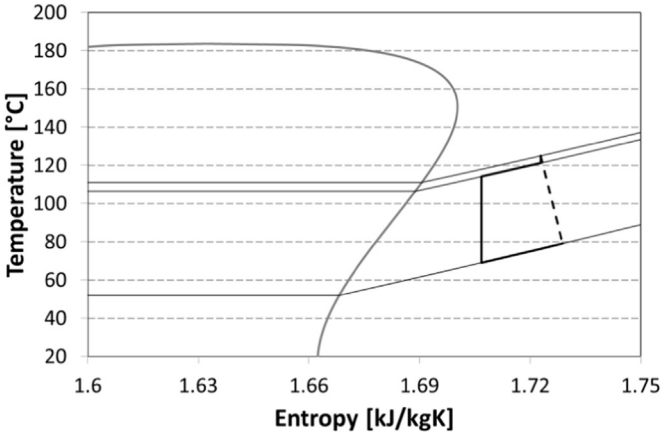

Fig. 4. T–s diagram with adapted expansion of HCFC-123 ($p_{su} = 1$ MPa, $T_{su} = 125$ °C, $\beta = 4.43$, $n = 2000$ rpm): solid thick lines trace the process simulated for each expansion stage whereas a dashed line connects the thermodynamic states of the fluid at the inlet and the outlet of the expander.

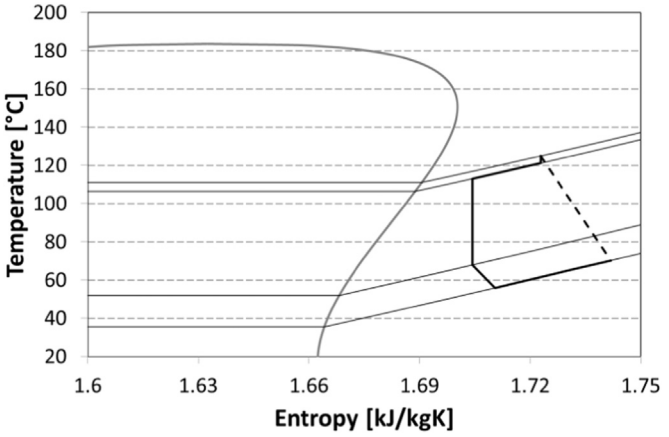

Fig. 5. T–s diagram with under-expansion of HCFC-123 ($p_{su} = 1$ MPa, $T_{su} = 125$ °C, $\beta = 7.5$, $n = 2000$ rpm): solid thick lines trace the process simulated for each expansion stage whereas a dashed line connects the thermodynamic states of the fluid at the inlet and the outlet of the expander.

AU_{amb} is not dependent on the working fluid as it simulates heat losses from the casing to the surroundings.

In particular, the thermal transmittance is calculated as

$$U = \frac{\mathrm{Nu}\cdot\lambda}{L} \tag{13}$$

where both Nusselt number and conductivity depend on the working fluid. Nusselt number is here calculated according to the commonly used Dittus-Boelter correlation [22]:

$$\mathrm{Nu} = 0.023\cdot \mathrm{Re}^{0.8}\cdot \mathrm{Pr}^{m} \tag{14}$$

The exponent m is equal to 0.4 if the fluid is heated by the wall, otherwise it is equal to 0.3 (the fluid is cooled by the wall). Reynolds and Prandtl numbers are notoriously formulated as

$$\mathrm{Re} = \frac{\rho\cdot w\cdot \mathrm{D}}{\mu} \tag{15}$$

$$\mathrm{Pr} = \frac{c_p\cdot\mu}{\lambda} \tag{16}$$

In this work, Eq. (14) was used for its easier application than more complex correlations, as the one provided by Gnielinski [27], considering that, in turbulent flow, the exponent of *Re* is dependent on the Prandtl number.

Both characteristic length and hydraulic diameter in Eqs. (13) and (15) are geometric parameters of the scroll expander, whereas velocity w is related to flow passage areas and swept volumes. Thus, they do not depend on the working fluid. If heat transfer areas are taken into account, according to Eq. (13):

$$\frac{AU_{\mathrm{fluid}}}{AU_{HCFC-123}} = \frac{Nu_{\mathrm{fluid}}\cdot\lambda_{\mathrm{fluid}}}{Nu_{HCFC-123}\cdot\lambda_{HCFC-123}} \tag{17}$$

Finally, Eq. (17) is revised in the light of the Dittus-Boelter correlation:

$$\frac{AU_{\mathrm{fluid}}}{AU_{HCFC-123}} = \left(\frac{Re_{\mathrm{fluid}}}{Re_{HCFC-123}}\right)^{0.8}\cdot\left(\frac{Pr_{\mathrm{fluid}}}{Pr_{HCFC-123}}\right)^{m}\cdot\left(\frac{\lambda_{\mathrm{fluid}}}{\lambda_{HCFC-123}}\right) \tag{18}$$

and the adaptation of the scroll expander model to fluids other than HCFC-123 is possible after both parameters $AU_{su,nom}$ and $AU_{ex,nom}$ are re-calculated as

$$AU_{\mathrm{fluid}} = AU_{HCFC-123}\cdot\left(\frac{\rho_{\mathrm{fluid}}}{\rho_{HCFC-123}}\right)^{0.8}\cdot\left(\frac{\mu_{HCFC-123}}{\mu_{\mathrm{fluid}}}\right)^{0.8-m}\cdot\left(\frac{c_{p\ \mathrm{fluid}}}{c_{p\ HCFC-123}}\right)^{m}\cdot\left(\frac{\lambda_{\mathrm{fluid}}}{\lambda_{HCFC-123}}\right)^{1-m} \tag{19}$$

A more rigorous approach would have been possible if frictional losses in the original formulation were not simply modelled by means of a constant torque parameter [9]. As a matter of fact, a more detailed model for frictional losses, including both Coulomb and viscous friction terms, would have at least suggested, besides a constant torque loss, a contribution depending on both fluid viscosity and rotational speed. In this last case, a re-calculation of the mechanical losses might have been necessary, as a consequence of the substitution of HCFC-123 with another fluid.

Table 3
Supply and exhaust heat transfer coefficients determined according to Eq. (19) for some fluids.

Fluid	$AU_{su,nom}$ (W K^{-1})	$AU_{ex,nom}$ (W K^{-1})
HCFC-123	21.2	34.2
HCFC-141b	21.57	33.43
HFC-245ca	28.42	45.37
HFC-365mfc	32.57	50.77
HFE-245fa2	25.33	43.82
HFE-347mcc[a]	33.03	52.56
HCFO-1233zd(E)	21.06	34.68
i-pentane	28.1	44.01
n-pentane	27.92	43.46

[a] Alias HFE-7000.

Table 4
Environmental data of the working fluids.

Fluid	ODP[a]	GWP[b]	ALT (yr)
HCFC-123	0.02	77	1.3
HCFC-141b	0.12	725	9.3
HFC-365mfc	0	794	8.6
HFE-245fa2	0	659	4.9
HFE-347mcc[c]	0	370	4.9
HFO-1233zd(E)	0	4.9	0.07

[a] Relative to CFC-11.
[b] Relative to CO_2 for a 100 year time horizon.
[c] Alias HFE-7000.

4. Calculation tools

The scroll expander model was implemented in the MATLAB environment, whereas the thermodynamic and transport properties of the working fluids were calculated by means of REFPROP, as developed by the National Institute of Standards and Technology of the United States [28].

According to the procedure detailed in the previous section, fluid transport properties are necessary to calculate new parameters for heat transfer when changing the working fluid. Later, simulations of the scroll expander performance may be run. In particular, the supply and exhaust heat transfer coefficients reported in Table 3 for a number of fluids were calculated with reference to supply pressure and temperature of 1003 kPa and 142 °C, an exhaust pressure of 201 kPa and a rotational speed of 2296 rpm, which is a specific measured performance point in Ref. [9].

5. Performance analysis

Simulation results of the scroll expander performance are presented in this section. The analysis focuses on six refrigerant fluids, taken as examples, even though the tool is general for any fluid with respect of the limitations reported in Table 2.[2] Two HCFCs are included in the analysis, in spite of HCFC phase-out regulations, just for their estimated higher performance [19]. On the other hand, four zero-ODP fluids are considered as well,[3] also including a specific environmentally friendly fluid [30], as detailed in Table 4.

Attention is first paid to the response of the model to the correction proposed in Section 3 by means of variations of the re-calculated heat transfer coefficients. Mass flow rate and power

[2] As an example, fixing a reference temperature of 100 °C for calculations, the corresponding saturation pressure for a zero-ODP fluid as HFC-134a is about 4 MPa, outside the range in Table 2.

[3] HFE-347mcc and Solkatherm® SES36 (an azeotropic mixture of HFC-365mfc) are indicated as alternatives to HCFC-123 [29].

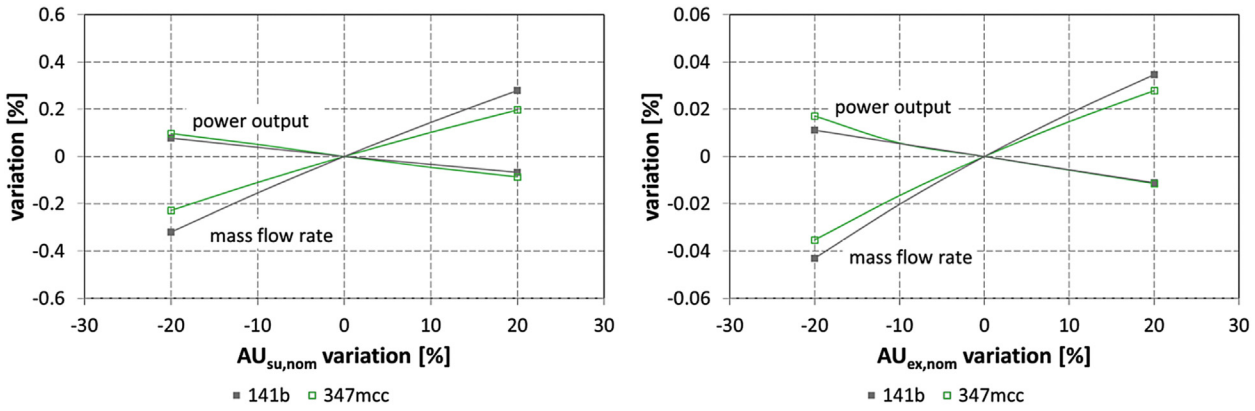

Fig. 6. Sensitivity of mass flow rate and power output on variations of supply and exhaust heat transfer coefficients (on the left and on the right, respectively).

output are here considered as main results of the model. Two cases are presented, when using HCFC-141b and HFE-347mcc, for the sake of simplicity, at the same operating point anticipated in Section 4. As a matter of fact, variations in supply and exhaust heat transfer coefficients ($AU_{su,nom}$ and $AU_{ex,nom}$) with respect to the ones in Table 3 clearly reflect on both terms $\dot{Q}_{su}$ and $\dot{Q}_{ex}$, necessary to determine ambient heat losses according to Eq. (11). However, $AU_{su,nom}$ and $AU_{ex,nom}$ variations in the range from −20% to 20% affect the $\dot{Q}_{amb}$ term no more than 1.5% or 3%, for the cases with HFE-347mcc and HCFC-141b respectively, and the final effects on mass flow rate and power output are really limited, as shown in Fig. 6. Likewise, Cuevas et al. [31] found really negligible disturbs of the response of their model against variations of the heat transfer coefficients for the case of a scroll compressor modelled according to an approach very similar to the one presented in Section 2.

Before presenting the results of expander performance simulations, this generalized mathematical modelling is here preliminarily verified against the results of previous experimental studies: the expander efficiency is used as the mean of comparison. According to the overview of experimental studies on scroll expanders as reported by Declaye et al. [6], the comparison between efficiency values as calculated with the proposed modelling and the experimental ones as reported in literature for similar positive-displacement expanders is good. On the other hand, expander efficiency depends on both fluid pressure and temperature at inlet, pressure ratio and rotational speed, so a more careful comparison should be based on similar operating conditions. Thus, referring to a specific operating condition as reported by Declaye et al. in their experimental work [6] for another small-size scroll expander, Fig. 7 shows efficiency vs. pressure ratio for cases regarding the four zero-ODP fluids in Table 4. A good efficiency trend may be appreciated, especially with reference to the maximum efficiency value.

Figs. 8 and 9 present comparisons between mass flow rates and power outputs calculated by means of the new generalized model for a range of rotational speeds. In particular, two temperatures at both the evaporator (100 °C) and the condenser (40 °C) were fixed, along with 10 °C of superheating for the working fluid at the expander inlet.[4] Thus, the state of the fluid at the inlet of the expander is fixed and the expansion pressure ratio is univocally determined, as reported in Table 5 for completeness.

As shown in Fig. 8, different mass flow rates were calculated depending on the working fluid. As a matter of fact, higher fluid

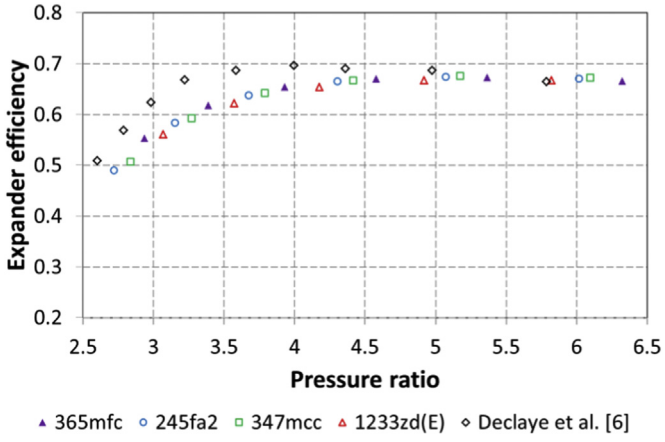

Fig. 7. Comparison between simulated expander efficiency and experimental literature data [6] for a specific operating condition (p_{su} = 900 kPa, ΔT_{su} = 10 K, n = 2500 rpm).

density at expander inlet brings about an increase in mass flow rate necessary to run the expander at the same rotational speed, as anticipated by Eq. (4). This result partly reflects on the power output at fixed rotational speed, since the mechanical power directly depends on the mass flow rate. Thus, it is possible to justify the results in Fig. 9, even though both the enthalpy drop through the expander and the ambient heat losses must be taken into account, as suggested by the first law of thermodynamics:

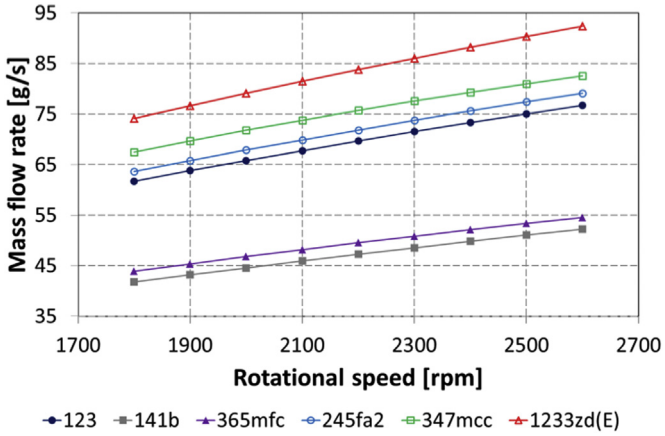

Fig. 8. Mass flow rate as a function of rotational speed (the thermodynamic operating condition is detailed in Table 5).

[4] Fluid superheating was considered since all of the performance points in [9] were determined for superheated conditions of the fluid supply, as reported in Table 2.

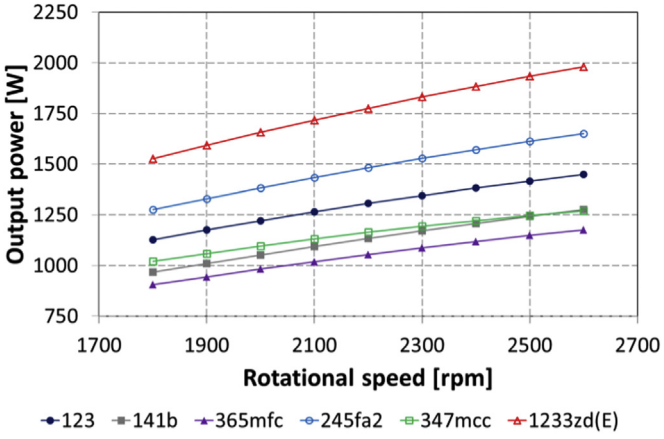

Fig. 9. Expander power as a function of rotational speed (the thermodynamic operating condition is detailed in Table 5).

Table 5
Supply pressure and density, expansion pressure ratio and latent heat of evaporation for the cases detailed in Figs. 8 and 9.

Fluid	p_{su} (kPa)	ρ_{su} (kg m^{-3})	β	Δh_{eva} (kJ kg^{-1})
HCFC-123	786	44.72	5.09	134.01
HCFC-141b	677	28.41	5.1	184.82
HFC-365mfc	587	31.64	5.83	154.04
HFE-245fa2	823	46.67	5.5	140.05
HFE-347mcc[a]	682	52.71	5.48	100.78
HFO-1233zd(E)	1042	53.01	4.84	142.46

[a] Alias HFE-7000.

$$P_{sh} = \dot{m} \cdot (h_{su} - h_{ex}) - \dot{Q}_{amb} \tag{20}$$

The effects of higher fluid temperatures at expander inlet could be significant since fluid expansion cannot be considered adiabatic in positive-displacement machines (it is diabatic even in radial-flow turbomachines [32]).

Fig. 10 shows power output, mass flow rate, enthalpy drop and ambient heat losses for cases of superheated fluid at fixed evaporation and condensation temperatures (100 °C and 40 °C, respectively) and rotational speed (2500 rpm). As reported in Fig. 10a, power output does not seem to depend on fluid superheating for the specified operating conditions. As a matter of fact, the mass flow rate decreases because of reduced supply fluid density, but both enthalpy drop and ambient heat losses increase. Moreover, calculations revealed negligible relative variations of scroll expander efficiency (less than 1% for the limit values of superheating, 110 °C and 140 °C), so the dependence of expander efficiency on supply superheating might be not significant. Such consideration is consistent with the results of Declaye et al. [6], who have recently highlighted the dependence of the efficiency of an open-drive scroll expander on supply pressure, pressure ratio and rotational speed, but not on the fluid temperature at the expander inlet. Nevertheless, ambient losses in Fig. 10d are worth of attention. Focusing on the highest superheating temperature, which reflects on higher envelope temperatures (T_w), ambient heat losses increase up to 40–45% (depending on the working fluid). In detail, they amount to 19–35% of the power output at 110 °C but raise to 27–47% at 140 °C. These results get worse at lower rotational speeds, when both the fluid mass flowing through the expander

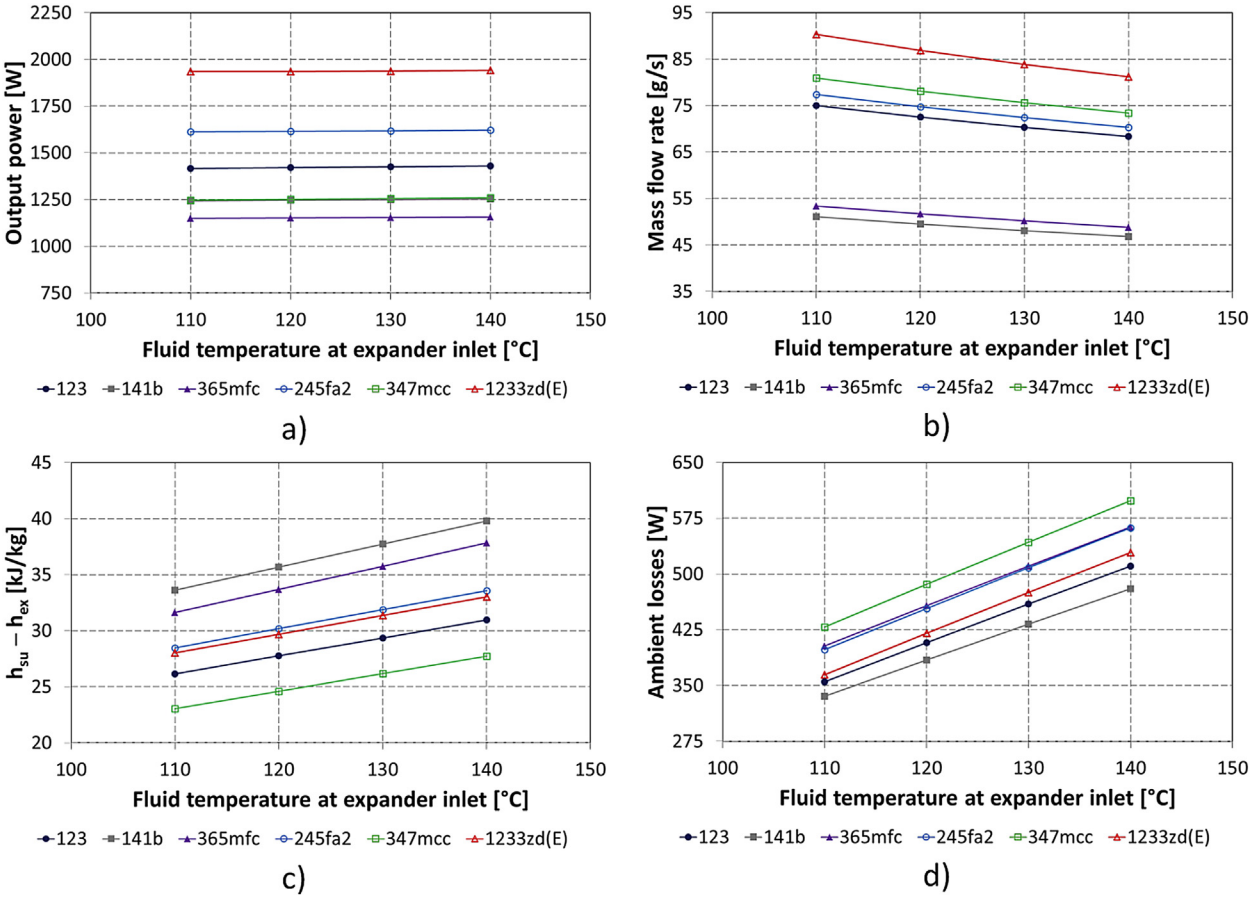

Fig. 10. Power output, mass flow rate, enthalpy drop and ambient heat losses depending on fluid superheating at expander inlet.

and the power output reduce, as previously shown in Figs. 8 and 9. As a matter of fact, reductions in mass flow rate reflect on both supply and exhaust heat transfers, as in Eq. (2), consequently on ambient heat losses, as in Eq. (11). However, reductions in heat losses are less than reductions in both mass flow rate and power output at lower rotational speeds. In particular, when repeating the same calculations at 1800 rpm, ambient losses increase up to 39–44%, if the highest superheating temperature is considered, and amount to 24–44% of the power output at 110 °C and raise to 34–61% at 140 °C. Of course, such results really affect the expander efficiency, which reduces at lower speeds for these specific operating conditions.

After performance comparisons of the scroll expander supplied with different fluids under specific operating conditions, the potential of this expander included in a few kW-size ORC system was investigated as well. In particular, without considering any specific application, which is outside the scope of the current work, some preliminary calculations of an ORC system were performed based on simple assumptions: (i) fluid condensation at 40 °C, (ii) no pressure drop from the pump outlet to the expander inlet and from the expander outlet to the pump inlet, (iii) saturated liquid at the inlet of the pump and (iv) pump efficiency equal to 0.5, as a reasonable average value among the results of Lin [33]. The ORC layout and a *T*–*s* diagram for HCFC-123 are reported in Fig. 11 for completeness. The ratio between net cycle power output and heat received by the fluid flowing from the pump outlet to the expander inlet returns the cycle efficiency, which is plotted in Figs. 12–14 for the previously considered six fluids. In particular, fluid temperature at the expander inlet was fixed 10 °C higher than the corresponding evaporation temperature in all calculations, even though fluid superheating does not always lead to higher efficiency for all working fluids [34]. As for the rotational speed, the range in Table 2 is here extended from 1500 to 3000 rpm in order to facilitate further considerations. Fluid evaporation temperature is chosen as the independent variable and set to maintain fixed expander power output at 1, 1.5 and 2 kW.

Looking at Figs. 12–14, the following results may be appreciated.

- Rotational speeds of the expander shaft equal to 1500 and 3000 rpm characterize the performance points on the right and left limits of each curve, respectively. As a matter of fact, lower evaporation temperatures, along with fixed condensation conditions, entail reduced expansion pressure ratios, i.e. reduced specific works, so an increase in flow rate, i.e. higher rotational speeds, is necessary to deliver the same power output.
- Higher values of evaporation temperature, i.e. higher expansion pressure ratios, are necessary to deliver more power.

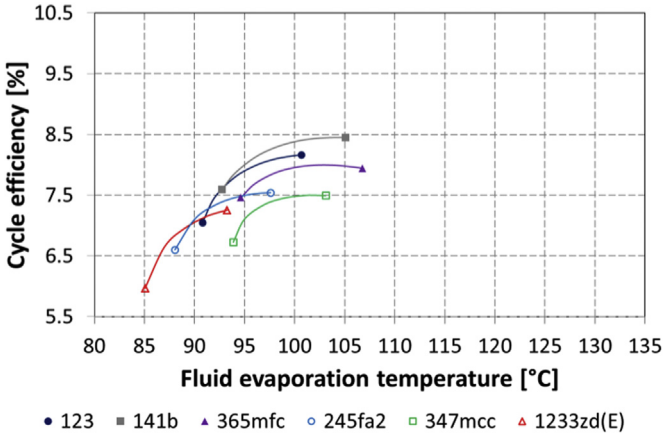

Fig. 12. ORC efficiency as a function of fluid evaporation temperature set for a scroll expander power equal to 1 kW.

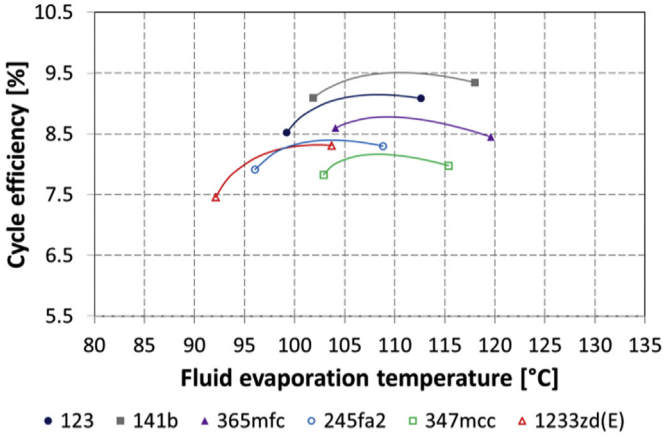

Fig. 13. ORC efficiency as a function of fluid evaporation temperature set for a scroll expander power equal to 1.5 kW.

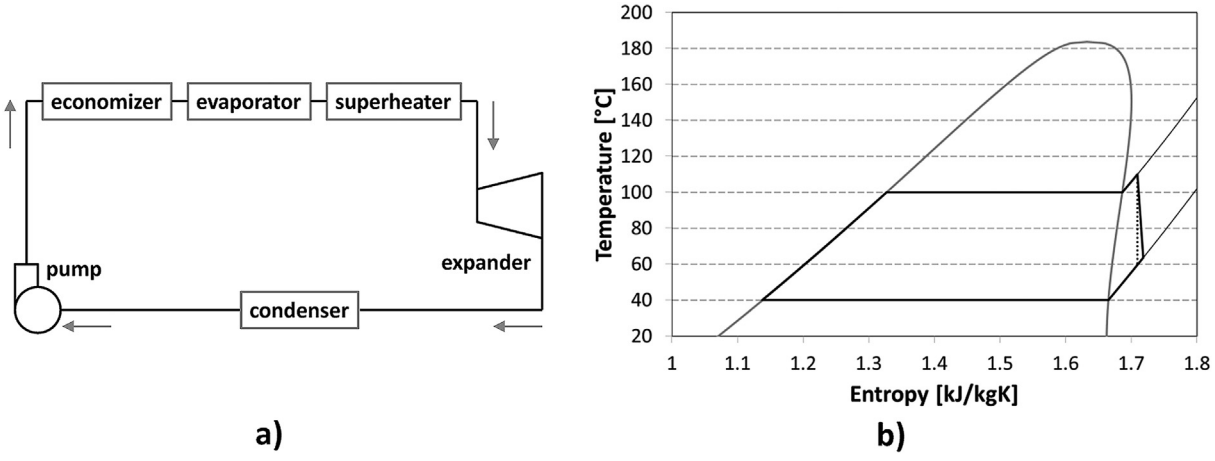

Fig. 11. Common ORC layout with main components (on the left) and its representation on a *T*–*s* diagram for HCFC-123 (on the right).

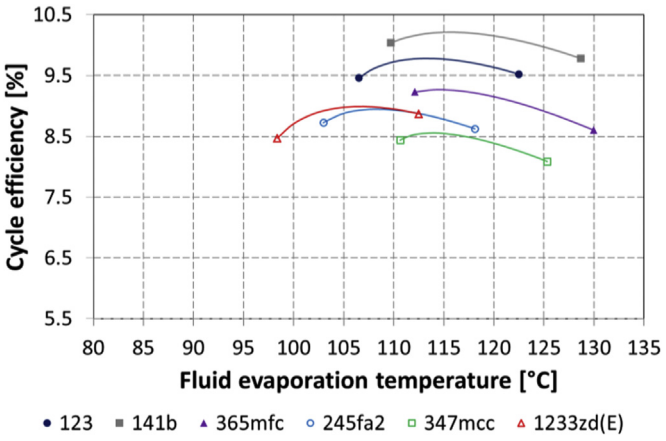

Fig. 14. ORC efficiency as a function of fluid evaporation temperature set for a scroll expander power equal to 2 kW.

- Cycle efficiency improves when power output is higher, since each curve moves to the upper right corner.
- Considering the same evaporation temperature, changes in rotational speed result in significant power output variations, as previously reported in Fig. 9. Nevertheless, the lower rotational speed, with the corresponding fluid evaporation temperature, should be selected for 1 kW of power output, but rotating at intermediate speed between 1500 and 3000 rpm seems to be more favorable when the power output is 1.5 and 2 kW, from the standpoint of cycle efficiency.
- Although the evaporation temperature ranges vary for each fluid, the highest cycle efficiency is achieved with HCFC-141b. Intermediate values were calculated for HCFC-123 and HFC-365mfc, even though the former seems to be more performant. Cycle efficiency trends for these three fluids are clear. A bit lower efficiency characterizes the other three cases, but the trends are worth of attention. Looking at Fig. 12, the case with HCFO-1233zd(E) presents the lowest efficiency, but higher values than the cases with HFE-245fa2 and HFE-347mcc seem to be possible for higher power outputs, as in Fig. 14. Moreover, the lower evaporation temperatures could be interesting in view of studying a low-temperature solar-based ORC system. Although the properties of HCFO-1233zd(E) are currently under study, the fluid is potentially interesting since it has (i) negligible ozone depletion potential, despite it has chlorine in the molecule, (ii) an extremely short atmospheric lifetime of 26 days and (iii) a global warming potential less than 5 [30].

6. Conclusions

Starting from an original scroll expander modelling for HCFC-123 [9], a thermodynamically realistic procedure was presented to generalize the model and to simulate the expander performance with fluids other than HCFC-123. In detail, considering that expander geometric parameters do not depend on the working fluid, the new model takes the correction of heat transfer coefficients into account, according to fluid density, viscosity, specific heat and thermal conductivity.

In detail, the new model was used here to simulate the mass flow rate necessary for a fixed rotational speed, as well as the related mechanical power output, and differences were highlighted when HCFC-123 is replaced by other working fluids.

Attention was also paid to heat losses, as fluid flow through the expander is not strictly adiabatic.

Ultimately, the proposed scroll expander model is useful for calculations of micro ORC systems, as it removes the assumption of adiabatic expander with constant isentropic efficiency, as usually adopted in literature works, in spite of the actual operating conditions of the expander. Although the proper working fluid should be selected according to the specific heat source, preliminary calculations suggested HCFC-141b is better than HCFC-123 from the standpoint of cycle efficiency. Nevertheless, considering HCFC phase-out regulations, the new HCFO-1233zd(E) was found to be a potentially interesting fluid in view of studying a low-temperature solar-based ORC system.

References

[1] S. Quoilin, M.V.D. Broek, S. Declaye, P. Dewallef, V. Lemort, Techno-economic survey of Organic Rankine Cycle (ORC) systems, Renew. Sustain. Energy Rev. 22 (2013) 168–186.
[2] G. Qiu, H. Liu, S. Riffat, Expanders for micro-CHP systems with organic Rankine cycle, Appl. Therm. Eng. 31 (2011) 3301–3307.
[3] V. Lemort, S. Declaye, S. Quoilin, Experimental characterization of a hermetic scroll expander for use in a micro-scale Rankine cycle, Proc. IMechE Part J. Power Energy 226 (2012) 126–136.
[4] www.orc2011.nl (accessed 14.11.13).
[5] www.asme-orc2013.nl (accessed 14.11.13).
[6] S. Declaye, S. Quoilin, L. Guillaume, V. Lemort, Experimental study on an open-drive scroll expander integrated into an ORC (Organic Rankine Cycle) system with R245fa as working fluid, Energy 55 (2013) 173–183.
[7] N. Zhou, X. Wang, Z. Chen, Z. Wang, Experimental study on Organic Rankine Cycle for waste heat recovery from low-temperature flue gas, Energy 55 (2013) 216–225.
[8] B. Twomey, P.A. Jacobs, H. Gurgenci, Dynamic performance estimation of small-scale solar cogeneration with an organic Rankine cycle using a scroll expander, Appl. Therm. Eng. 51 (2013) 1307–1316.
[9] V. Lemort, S. Quoilin, C. Cuevas, J. Lebrun, Testing and modeling a scroll expander integrated into an organic Rankine cycle, Appl. Therm. Eng. 29 (2009) 3094–3102.
[10] J.F. Oudkerk, S. Quoilin, S. Declaye, L. Guillaume, E. Winandy, V. Lemort, Evaluation of the energy performance of an organic Rankine cycle-based micro combined heat and power system involving a hermetic scroll expander, J. Eng. Gas. Turbines Power 135 (4) (2013) article number 42306.
[11] S. Clemente, D. Micheli, M. Reini, R. Taccani, Energy efficiency analysis of Organic Rankine Cycles with scroll expanders for cogenerative applications, Appl. Energy 97 (2012) 792–801.
[12] R. Bracco, S. Clemente, D. Micheli, M. Reini, Experimental tests and modelization of a domestic-scale ORC (Organic Rankine Cycle), Energy 58 (2013) 107–116.
[13] G. Kosmadakis, D. Manolakos, G. Papadakis, An investigation of design concepts and control strategies of a double-stage expansion solar organic Rankine cycle, Int. J. Sustain. Energy (2013), http://dx.doi.org/10.1080/14786451.2013.827682.
[14] M. Jradi, S. Riffat, Modelling and testing of a hybrid solar-biomass ORC-based micro-CHP system, Int. J. Energy Res. 38 (8) (2014) 1039–1052.
[15] M. Ibarra, A. Rovia, D.C. Alarcón-Padilla, J. Blanco, Performance of a 5 kW_e Organic Rankine Cycle at part-load operation, Appl. Energy 120 (2014) 147–158.
[16] H. Liu, Y. Shao, J. Li, A biomass-fired micro-scale CHP system with organic Rankine cycle (ORC) – thermodynamic modelling studies, Biomass Bioenergy 35 (2011) 3985–3994.
[17] B. Saleh, G. Koglbauer, M. Wendland, J. Fischer, Working fluids for low-temperature Organic Rankine Cycles, Energy 32 (2007) 1210–1221.
[18] B.F. Tchanche, G. Papadakis, G. Lambrinos, A. Frangoudakis, Fluid selection for a low-temperature solar organic Rankine cycle, Appl. Therm. Eng. 29 (2009) 2468–2476.
[19] D. Mikielewicz, J. Mikielewicz, A thermodynamic criterion for selection of working fluid for subcritical and supercritical domestic micro CHP, Appl. Therm. Eng. 30 (2010) 2357–2362.
[20] D. Wang, X. Ling, H. Peng, L. Liu, L. Tao, Efficiency and optimal performance evaluation of organic Rankine cycle for low grade waste heat power generation, Energy 50 (2013) 343–352.
[21] H. Xi, M.J. Li, C. Xu, Y.L. He, Parametric optimization of regenerative organic Rankine cycle (ORC) for low grade waste heat recovery using genetic algorithm, Energy 58 (2013) 473–482.
[22] F.P. Incropera, P.D. De Witt, T.L. Bergman, A.S. Lavine, Introduction to Heat Transfer, fifth ed., John Wiley & Sons, 2007.
[23] S.A. Korpela, Principles of Turbomachinery, first ed., John Wiley & Sons, 2011.
[24] Byrne P., Ghoubali R., Miriel J, Development of a Scroll Compressor Model for Propane, Proceedings of the 10th IIR Gustav Lorentzen Conference on Natural Refrigerants, June 25–27, 2012, Delft, The Netherlands.
[25] P. Byrne, R. Ghoubali, J. Miriel, Scroll compressor modelling for heat pumps using hydrocarbons as refrigerants, Int. J. Refrig. 41 (2014) 1–13.

[26] M.E. Duprez, E. Dumont, M. Frère, Modeling of scroll compressors – improvements, Int. J. Refrig. 33 (2010) 721–728.
[27] V. Gnielinski, On heat transfer in tubes, Int. J. Heat. Mass Transf. 63 (2013) 134–140.
[28] www.nist.gov/srd/nist23.cfm (accessed 14.11.13).
[29] S. Quoilin, S. Declaye, B.F. Tchanche, V. Lemort, Thermo-economic optimization of waste heat recovery Organic Rankine Cycles, Appl. Therm. Eng. 31 (2011) 2885–2893.
[30] R.J. Hulse, R.S. Basu, R.R. Singh, R.H.P. Thomas, Physical properties of HCFO-1233zd(E), J. Chem. Eng. Data 57 (12) (2012) 3581–3586.
[31] C. Cuevas, J. Lebrun, V. Lemort, E. Winandy, Characterization of a scroll compressor under extended operating conditions, Appl. Therm. Eng. 30 (6-7) (2010) 605–615.
[32] A. Romagnoli, R. Martinez-Botas, Heat transfer analysis in a turbocharger turbine: an experimental and computational evaluation, Appl. Therm. Eng. 38 (2012) 58–77.
[33] C. Lin, Feasibility of Using Power Steering Pumps in Small-Scale Solar Thermal Electric Power Systems, Massachusetts Institute of Technology, 2008, pp. 1–70 (S.B. thesis).
[34] H. Chen, D.Y. Goswami, E.K. Stefanakos, A review of thermodynamic cycles and working fluids for the conversion of low-grade heat, Renew. Sustain. Energy Rev. 14 (9) (2010) 3059–3067.

Glossary

A: area, m^2
AU: heat transfer coefficient, W K^{-1}
c: specific heat, J kg^{-1} K^{-1}
D: hydraulic diameter, m
h: specific enthalpy, J kg^{-1}
L: length, m
$\dot{m}$*:* mass flow rate, kg s^{-1}
n: rotational speed, rpm
Nu: Nusselt number
p: pressure, Pa
P: power, W
Pr: Prandtl number
$\dot{Q}$*:* heat transfer rate, W
Re: Reynolds number
s: specific entropy, J kg^{-1} K^{-1}
T: temperature, °C
U: thermal transmittance, W m^{-2} K^{-1}
v: specific volume, m^3 kg^{-1}
V: volume, m^3
w: velocity, m s^{-1}
β*:* pressure ratio
γ*:* isentropic exponent
Δ*:* difference
η*:* efficiency
λ*:* thermal conductivity, W m^{-1} K^{-1}
μ*:* dynamic viscosity, Pa s
ρ*:* density, kg m^{-3}
τ*:* torque, N m

Subscripts

ad: adapted
amb: ambient
crit: critical
el: electric
ex: exhaust
in: internal
is: isentropic
leak: leakage
loss: mechanical loss
nom: nominal
p: constant pressure
sh: shaft
su: supply
sw: swept
w: envelope

Acronyms

ALT: atmospheric lifetime
BVR: built-in volume ratio
CFC: chlorofluorocarbon
CHP: combined heat and power
GWP: global warming potential
HCFC: hydroclorofluorocarbon
HCFO: hydrochlorofluoroolefin
HFC: hydrofluorocarbon
HFE: hydrofluoroether
HVAC: heating, ventilation, and air conditioning
ODP: ozone depletion potential
ORC: organic Rankine cycle